Is it possible to measure the tensile strength and fracture toughness simultaneously using flattened Brazilian disk?

Haiyang Yu[a,b,*], Dag Herman Andersen[a,c], Jianying He[a], Zhiliang Zhang[a]

[a] *Department of Structural Engineering, Norwegian University of Science and Technology, 7491 Trondheim, Norway*
[b] *Department of Materials, University of Oxford, Parks Road, OX1 3PH, UK*
[c] *Norsk Hydro, Technology & Operational Support, NO-6882 Øvre Årdal, Norway*

Abstract

The Flattened Brazilian Disk test was designed for measuring both the tensile strength and fracture toughness of rocks. Using cohesive zone modelling, we found that the method is practically not suitable for extracting the fracture toughness, while it works well in calibrating the tensile strength. The flattened Brazilian disk provides a very narrow window for the variation of load during failure, $< 15\%$, insufficient to reflect the change in fracture toughness among different materials. The crack propagation throughout failure is highly unstable and dynamic, where linear elastic fracture mechanics is not applicable. These findings were supported by experimental data. In contrast, the Semi-Circular Bend test, with a pre-crack, can properly measure the fracture toughness but cannot capture the change in the tensile strength. In general, un-cracked disk specimens are suitable for measuring the tensile

*Corresponding author
Email addresses: haiyang.yu@materials.ox.ac.uk (Haiyang Yu), jianying.he@materials.ox.ac.uk (Jianying He), zhiliang.zhang@ntnu.no (Zhiliang Zhang)

strength and pre-cracked specimens for the fracture toughness. It is very challenging, if not impossible, to measure both with a single test. It is further implied that the first peak on the loading curve in such kind of tests is trustworthy for extracting mechanical properties, while the following second turning point (if existing) is unreliable as it may contain dynamic effect. These results provide useful reference for the selection and design of test methods using Brazilian disk related geometries.
Keywords: Flattened Brazilian Disk, Semi-Circular Bend Specimen, Fracture toughness, Cohesive zone modelling

1. Introduction

The tensile strength and fracture toughness are key parameters governing the failure properties of brittle materials such as rocks. Due to the brittle nature, it is hard to measure these properties directly using tensile tests [1]. The Brazilian disk test is a well established indirect method for calibrating these properties. A circular disk is subjected to compression, which triggers tensile failure at the center of the specimen, the tensile properties can then be deduced from the loading curves based on linear elastic fracture mechanics (LEFM) theory [2]. Theoretically this geometry can be used to extract both the tensile strength and fracture toughness. Hondros [2] gave the complete stress solution under an arc load, and Guo et al. [3] proposed a formulation to extract the fracture toughness. This method however has practical drawbacks. Wang and Xing [4] pointed out that the primary crack initiation at the centre region of the Brazilian disc during the test was a key problem

which cannot be guaranteed in practice. Failure initiated close to the loading platens [5] also undermines the accuracy of the test.

In the past decades, a large amount of research has been conducted on Brazilian disk test methods, endeavouring to increase the accuracy and/or reduce the complexity of the calibration. Fowell and Xu [6], Fowell [7] utilized a cracked chevron notched Brazilian disk (CCNBD) geometry to extract the mode I fracture toughness, a formula was derived relating the fracture toughness to the maximum load on the loading curve. This approach guarantees crack initiation from the notch and benefits from a higher failure load which usually means better accuracy. A more accurate calibration of the minimum dimensionless stress intensity factor was given by Wang et al. [8]. A similar approach which also uses the maximum load to calculate the fracture toughness is the Semi-Circular Bend Specimen (SCB) [9]. A typical loading curve in a SCB test is illustrated in Fig. 1(a). Wang et al. [10] in-

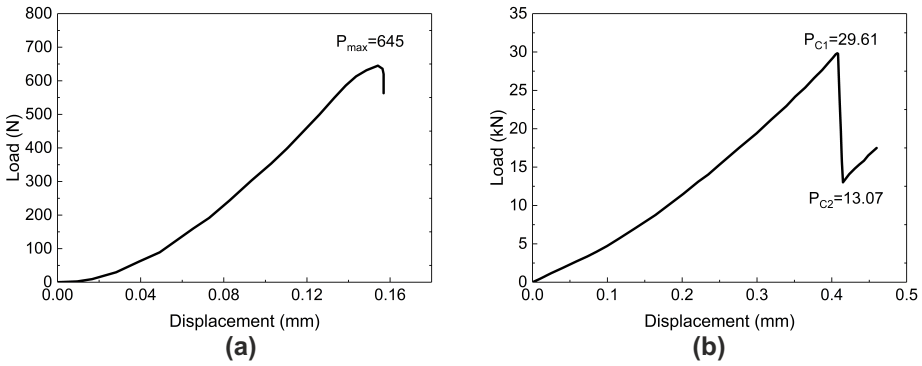

Fig. 1 (a) A typical loading curve in a SCB test, reproduced from [9] and (b) a typical loading curve in a FBD test, reproduced from [10].

troduced a flattened Brazilian disk (FBD) method which guarantees central crack initiation when the flat end is longer than a critical value. The tensile

strength can be extracted from the load at the first peak of the loading curve which corresponds to crack initiation. This specimen is easy to prepare and the application of load is convenient. Fowell et al. [11] reviewed the FBD geometry and compared it with other existing methods. Huang et al. [12] used the FBD test to measure the tensile strength of rocks, pointing out that the optimal flattened loading angle was $20-30^{\circ}$ and that angles too large or too small violated the central tensile splitting failure principle. Wang et al. [10] claimed that the mode I fracture toughness can be extracted from the same FBD test, which is a major advantage of this method. After failure initiation, the crack first propagates unstably and then stably towards the flat end, so the load drops following the first peak on the loading curve and then increases. Therefore, the fracture toughness can be calculated from the minimum load after the first peak. A typical loading curve in a FBD test is illustrated in Fig. 1(b). However, the effectiveness of this method in calibrating the fracture toughness has not been rigorously validated [11, 13]. According to Keles and Tutluoglu [14], the FBD test could give overestimation of the fracture toughness compared to the ISRM suggested CCNBD method.

We recently employed the FBD method to test the fracture properties of pre-baked carbon anodes for aluminum production, considering the advantage that the tensile strength and fracture toughness can be obtained within a single test. The specimens were manufactured as recommended in [10] with a loading angle $\alpha = 30^{\circ}$. The method gave sensible value of tensile strength but overestimated the fracture toughness. We then revisited the FBD method with cohesive zone modelling (CZM) approach. CZM is an ideal approach

to modelling material failure featured by a fracture process zone (FPZ) [15]. Comparison between CZM and the classical fracture mechanics was made by Jin and Sun [16], Wang [17]. On condition that the size of FPZ is small relative to the crack length, the stress field of CZM approaches that of LEFM, and these two can be regarded equivalent. So CZM can be used to reproduce and verify the LEFM based models. Inconsistency was found between our CZM simulation and the FBD model. The variation in the cohesive energy, thus the fracture toughness, could not be properly reflected on the loading curves of the simulated FBD tests. The major issue with the FBD test was shown to be the crack propagating in a highly dynamic manner after failure so the assumption that the applied stress intensity factor equals the fracture toughness is not appropriate, which is elaborated in section 4.

To find an alternative approach to measuring the fracture toughness, we analysed the SCB method and verified that it is consistent with the CZM results. The SCB test, however, is not suitable for measuring the tensile strength, in contrast to the FBD test. Based on these results, we further discussed the suitability of using the reference points, i.e. the maximum load and the turning point following the first peak, to extract the mechanical properties. With these aspects elaborated, we gave our answer to the question whether it is possible to measure both the tensile strength and fracture toughness with a single test.

2. Models

Failure in rock like material is mostly brittle, so the models for fracture toughness calibration are usually based on LEFM. Using dimensional analy-

sis, the relation can be drawn between applied stress intensity factor K_I, the external load and geometric dimensions of the disk; by equating the fracture toughness K_{IC} to K_I at a proper point, K_{IC} can be extracted from the loading curve. Here we briefly review the FBD model and the SCB model which are concerned in this work.

2.1. The FBD model and the SCB model

The geometry of the FBD model is shown in Fig. 2(a). Two flat ends are introduced to the original Brazilian disk to enforce crack initiation from the disk centre. It was shown by Wang et al. [10] that the opening stress reaches its maximum at the centre and thus guarantees central failure initiation under the condition $2\alpha \geq 20°$. In this scenario, the tensile strength of the material

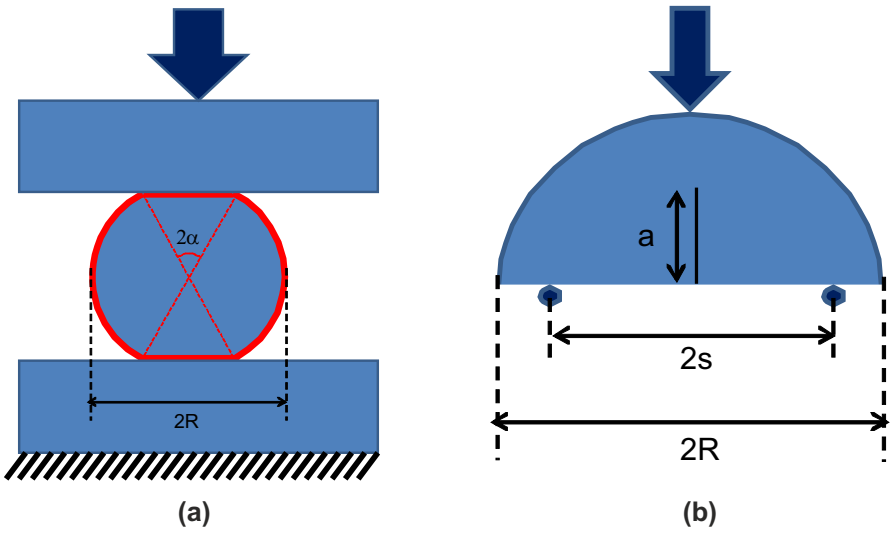

Fig. 2 Illustration of (a) the FBD test and (b) the SCB test.

is expressed as

$$\sigma_t = k\frac{2P_{C1}}{\pi Dt} \tag{1}$$

where P_{C1} is the force at the first peak on the loading curve, as shown in Fig. 1(b); k is a coefficient depending on the loading angle, $k = 0.9644$ for $2\alpha = 20°$ and $k = 0.9205$ for $2\alpha = 30°$; t is the thickness of the sample.

After failure, the crack propagates towards the end of the FBD. For a central through crack with length $2a$, the applied stress intensity factor is expressed as

$$K_I = \frac{P}{\sqrt{R}t}\Phi(\alpha, a/R) \tag{2}$$

where P is the applied force and R the radius of the disk. Φ is the dimensionless stress intensity factor, its variation with the growth of the crack was calibrated numerically, and the curve for the case $2\alpha = 30°$ is reproduced here in Fig. 3. Assuming that fracture toughness K_{IC} is a material constant and that $K_I = K_{IC}$, the fracture toughness can be determined at any moment during crack propagation [10]. Theoretically, the lower peak P_{C2} in Fig. 1(b) corresponds to the Φ_{max} in Fig. 3 and is therefore ideal for calculating the fracture toughness

$$K_{IC} = \frac{P_{C2}}{\sqrt{R}t}\Phi_{max}, \qquad \Phi_{max} = 0.5895 \quad for \quad 2\alpha = 30° \tag{3}$$

Equation 3 is theoretically sound, but there seems to be practical difficulty in its application. Under the assumption $K_I = K_{IC}$ as explicitly stated in [10], it directly gives $P_{C2}/P_{C1} = \Phi_{min}/\Phi_{max}$. According to Fig. 3, this ratio can be less than 1/5 if we take $\Phi_{min} = 0.1$ right after crack initiation, which is even smaller for cases with $2\alpha < 30°$. Such dramatic drop in the loading curve has never been recorded in FBD experiments [10, 13, 14, 18]. Extended discussion regarding this issue will be presented in the next section.

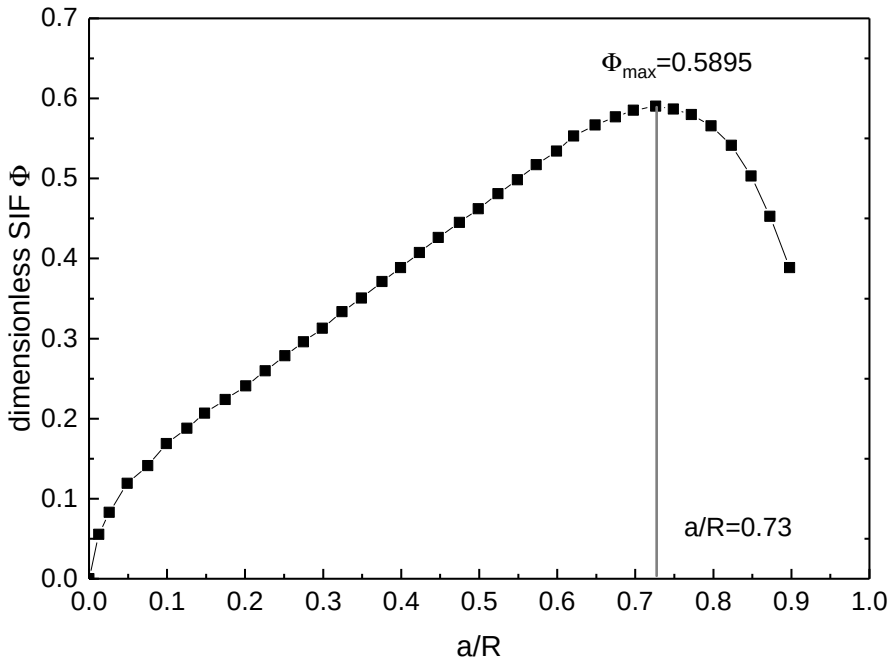

Fig. 3 The variation of dimensionless stress intensity factor with half central crack length, for the case with $2\alpha = 30°$. The figure is reproduced from [10].

The geometry of the SCB test is presented in Fig. 2(b). Based on LEFM and assuming $K_I = K_{IC}$ at the initiation of failure, the mode I fracture toughness is determined as [19]

$$K_{IC} = Y'(a, R, s)\frac{P_{max}\sqrt{\pi a}}{2RB} \tag{4}$$

where P_{max} is the peak on the loading curve as shown in Fig. 1(a), a the pre-existing crack length, R the radius of the disk, B the thickness and s the span length. $Y'(a, R, s)$ is the dimensionless stress intensity factor and was determined using the finite element method [9]. It was suggested that the test should be done at a constant displacement rate of not greater than

$0.2mm/min$ to avoid any dynamic effect.

Under the condition of quasi-static loading, the crack length a in Equation 4 is practically measurable (equal to the length of the pre-crack) in the SCB test, and little dynamic influence exists at the event of failure initiation. This is a major difference between the FBD and SCB methods in determining the fracture toughness.

2.2. Cohesive zone model

CZM is a phenomenological representation of interface separation during crack propagation, with a layer of cohesive elements inserted along the anticipated crack path between the solid elements representing the matrix, e.g. along the central ligament of the FBD and SCB specimens. The constitutive behavior of the cohesive element is described by the so-called traction separation law (TSL) characterized by the cohesive strength, σ_C and the critical cohesive separation δ_C [20]. Upon loading, the cohesive stress first increases until σ_C is reached, triggering material degradation (softening), complete failure of the element then occurs as the cohesive separation reaches δ_C. The area under the TSL curve represents the critical energy release rate also referred to as the cohesive energy G_C. The TSL can take several forms, and the simplest bi-linear form is adopted here, as illustrated in Fig. 4. In CZM there exists a near-tip process zone where the opening stress field is finite. When loaded, the cohesive element closest to the crack tip rapidly reaches its cohesive strength and moves on to the softening phase of the TSL; the adjacent cohesive elements also gradually develop to this phase. The region inside which cohesive elements are in the softening phase is defined as the failure process zone (FPZ), and the length of this zone is denoted l_{FPZ}. A

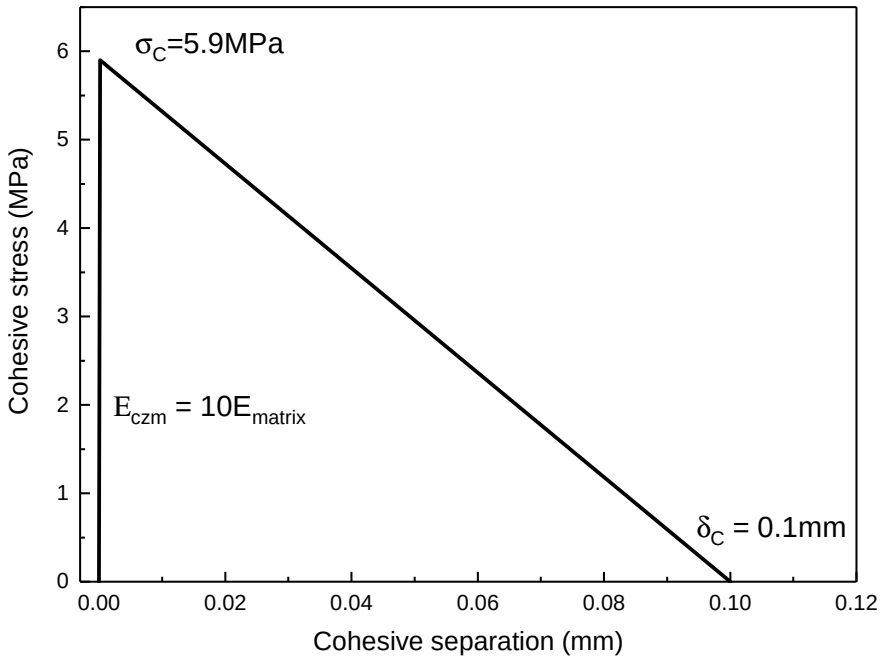

Fig. 4 A bilinear TSL with parameters used in one of the simulations in this work. The initial stiffness of the cohesive element E_{CZM} was set as $10\times$ the Young's modulus of the matrix material, E_{matrix}, in order to minimize the influence on the global stiffness [21].

detailed illustration of FPZ is found in [22]. Many studies were dedicated to estimating l_{FPZ} in different scenarios. Turon et al. [23] gave a summary of these studies and concluded that the models have the general form

$$l_{FPZ} = ME\frac{G_C}{\sigma_C^2} \tag{5}$$

where E is the effective Young's modulus of the matrix material and M a coefficient dependent on the TSL; $M = 0.21$ is adopted in this work following Hui et al. [24].

Here we use CZM as a flexible virtual experimental method to probe the effectiveness of the LEFM based models. For this purpose, we just need to tailor the modelling parameters such that l_{FPZ} is small compared to the characteristic dimension of the specimen, under which condition CZM results are approximately the same as LEFM results. CZM and LEFM are generally deemed applicable if a primary central crack is distinguishable in the disk after the test. In practice, secondary cracks and crack branching can also be observed. To model the complex cracking pattern, phase field modelling has proven an efficient tool [25, 26].

3. Experiment

We performed a series of FBD tests on pre-baked carbon anodes used in the electrolytic production of aluminum. The anodes were sampled in cylindrical shape with length of $170mm$ and diameter of $135mm$. General properties of this material are summarized in Table 1 [27, 28] (note that there was a mistake in [27], the Young's mdulus should be deducted by a half). Considering the convenient specimen preparation and especially the ability

Table 1 General properties of pre-baked carbon.

Density (g/cm^3)	1.54-1.63
Young's modulus $E(MPa)$	3500-5500
Tensile strength $\sigma_t(MPa)$	3.5-10.0
Fracture toughness $K_{IC}(MPa\sqrt{m})$	1.21-1.60
Fracture strain ε_C	0.06%-0.10%

to extract both the tensile strength and fracture toughness from a single test, the FBD method was adopted to calibrate the tensile properties for the

target material. In this round we tested 4 cylindrical samples, each cylinder was cut to three pieces with a thickness of $t = 50mm$, 12 in total, which were then manufactured to FBD specimens with a loading angle of $2\alpha = 30°$. Compression test was conducted using a standard Instron test system with appropriate load cell. Displacement-controlled loading with a constant displacement rate of 1 mm/min was applied. The load–displacement curve was recorded and the load was continued until the specimen fractured. The test is considered valid if a primary crack is observed in the central region of the disk and the first peak P_{C1} and second peak P_{C2} are clearly distinguishable on the loading curve. In this round of tests we had 9 valid ones. The loading curves and failed specimens in three typical tests, indexed S1, S2 and S3, are presented in Fig. 5. By extracting P_{C1} and P_{C2} from the loading curve and using Equation 3, the tensile strength and fracture toughness were obtained, as summarized in Table 2. The values for the tensile strength were

Table 2 Summary of the test results.

	S1	S2	S3
$P_{C1}(kN)$	69.96	72.97	78.70
$P_{C2}(kN)$	60.60	64.02	69.30
$E(MPa)$	3750	3850	4000
$\sigma_t(MPa)$	6.30	6.57	7.07
$K_{IC}(MPa\sqrt{m})$	2.84	3.00	3.24

reasonable, while the mode I fracture toughness seemed overestimated. To probe the reason, we interpreted the results with CZM. The simulations were performed via ABAQUS [29]. Due to symmetry, a quarter of the disk was modelled. The matrix was modelled with plane strain elements, 12006 in to-

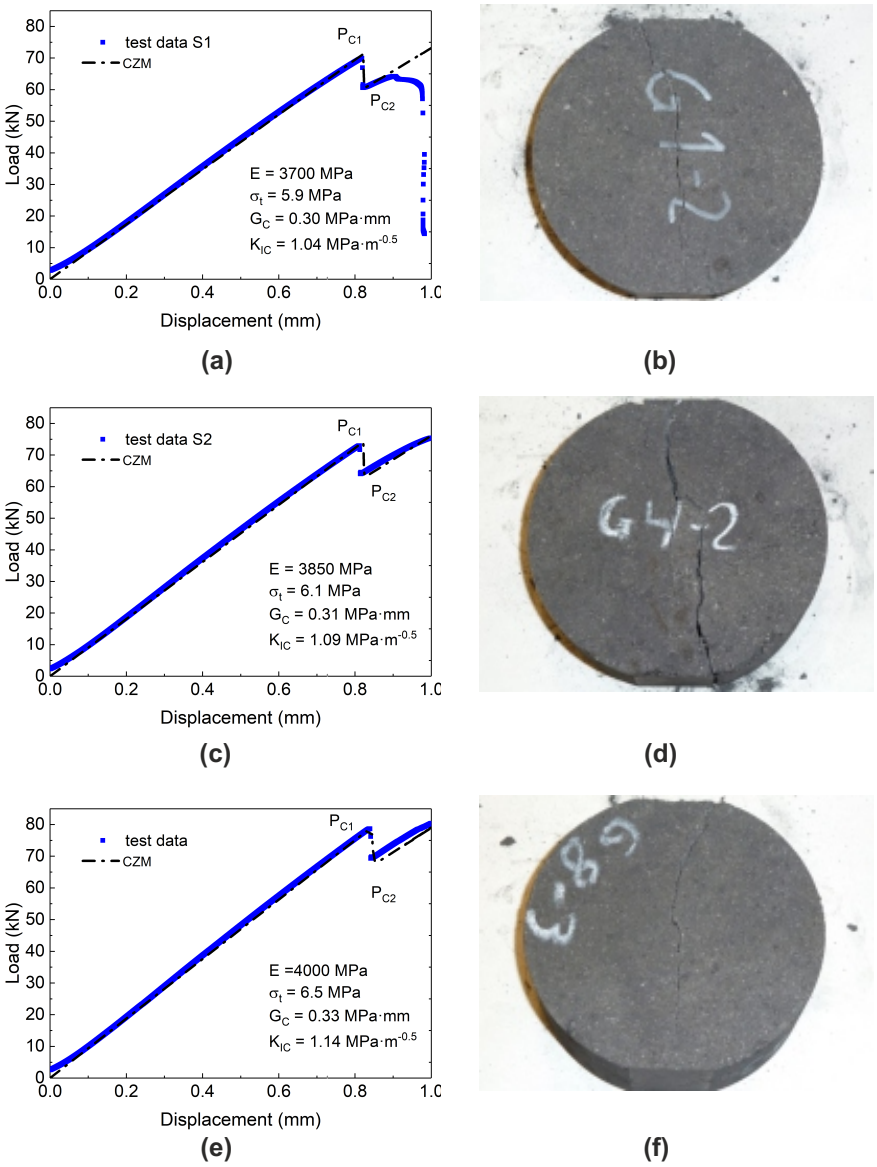

Fig. 5 (a) and (b) are respectively the loading curve and the final state of the specimen S1; (c) and (d) are respectively the loading curve and the final state of the specimen S2; (e) and (f) are respectively the loading curve and the final state of the specimen S3. The CZM simulated curves of the three tests and the modelling parameters are also included in sub-figures (a), (c) and (e), respectively.

tal. Contact with small glide was defined between a rigid plate and the disk, displacement was applied to the plate to simulate displacement controlled compression in the test. Crack is anticipated to initiate from the centre and propagate to the flat ends, so the central diameter of the disk was modelled with cohesive elements. Details regarding applying symmetry condition to CZM is found in [30]. To ensure sufficient resolution of the FPZ, the cohesive region was refined, given 500 elements in total. Bilinear TSL as shown in Fig. 4 was adopted. The results of the simulation are detailed in Fig. 5. To determine the cohesive parameters, we first estimated the elastic modulus of the material to be ≈ 4000 MPa; taking this value and considering the general properties of the target material as listed in Table 1, it could be estimated that the critical cohesive separation was in the magnitude of 0.1 mm; we therefore took the critical separation as $\delta_C = 0.1$ mm and varied the cohesive stress σ_C to fit the experimental loading curve; the fracture toughness was then naturally obtained upon determination of σ_C. In this process, it is noted that only σ_C was strictly fitted from the experiments, while δ_C was prescribed empirically. This is because it's actually only possible to determine σ_C but impossible to determine δ_C using the FBD test, which will be elaborated later in Fig. 7 in section 4. With the aforementioned parameter determining procedure, the test results are effectively captured, with a tensile strength σ_C in general agreement with the prediction by Equation 1 but a K_{IC} substantially smaller than predicted by Equation 3. Considering that the size of the FPZ is only a tenth of the specimen dimension, there should be good agreement between the CZM and LEFM results. The discrepancy observed here is unexpected and needs investigation.

4. Discussion

4.1. The FBD model

With CZM, it is possible to follow crack propagation. The first peak P_{C1} on the loading curve corresponded to failure initiation as expected, but the half crack length at the second point P_{C2} was found to be $a \approx 0.91R$. This is in contrast to Fig. 3 where P_{C2} is anticipated to occur at a half crack length of $a \approx 0.73R$. Further, it was observed that the crack length in CZM simulations increased only marginally with further loading beyond the second point P_{C2}. Also considering that the half crack length $a \approx 0.91R$ gives about 95% central ligament separation, we judge that the CZM specimen has completely failed at point P_{C2}. To support this, we simulated two simple cases without cohesive elements: 1) an intact FBD specimen and 2) a completely failed FBD specimen; the difference between these two lies in that the DOFs of the central line were set free in the latter case. The same mechanical parameters fitted for test S2 were applied to these cases and the results are plotted with the CZM loading curve in Fig. 6. This figure also sets the upper and lower limits for the load during an FBD test at a given displacement: the load cannot be smaller than that in the completely failed state indicated by the red dashed line. Apparently, the ratio between the lower and upper limit at the same displacement is constant for a given FBD specimen, we further found that this ratio is marginally dependent on the elastic properties, that is, varying the elastic modulus and Poisson's ratio has practically no influence on the ratio. In other words, given a geometry and assuming failure by central cracking, the P_{C2}/P_{C1} ratio is approximately constant, e.g. in the current case with $2\alpha = 30°$ we have $P_{C2}/P_{C1} \approx 0.85$. This value agrees with

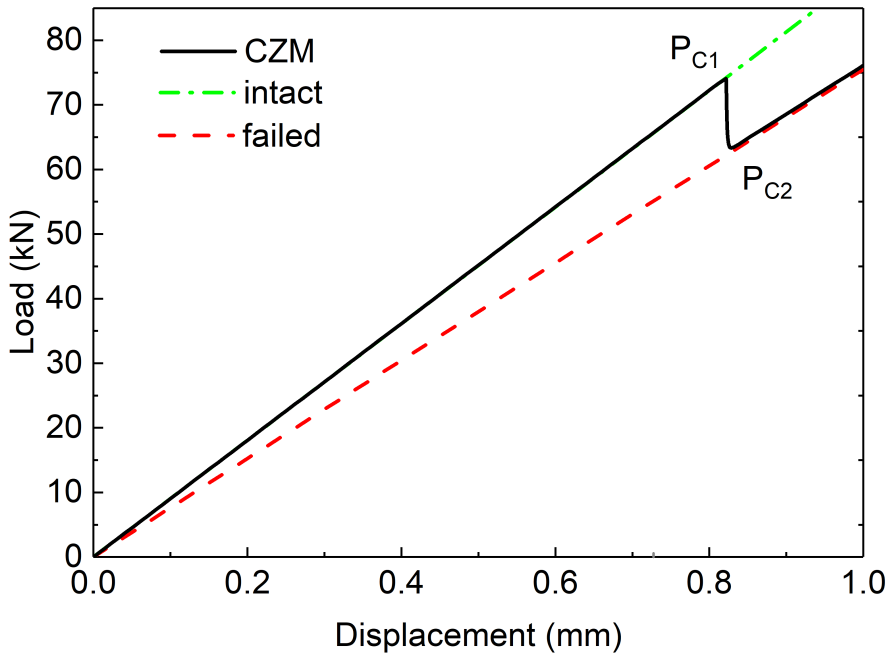

Fig. 6 CZM loading curve versus the compression of an intact FBD assuming no damage and a failed FBD assuming complete damage along the central ligament.

the test results.

According to Equation 1, P_{C1} is fixed given a tensile strength of the material. P_{C2} is then limited to a narrow range $(0.85P_{C1}, P_{C1})$, which is insufficient to distinguish the variation of fracture toughness among different materials. This can be directly demonstrated using CZM. To study the variation with tensile properties, we selected the parameters calibrated for test S2 in Fig. 5(c) as the reference and denote the tensile strength as σ_0, the mode I fracture toughness as K_{IC0} and the fracture energy as G_0. The cohesive parameters were then varied with respect to the reference. Keeping $\sigma_t = \sigma_0$ and decreasing G_C to $0.1G_0$, there was little change in P_{C2} as shown

in Fig. 7, while Equation 3 expects a 63.38% reduction in P_{C2} ($1 - \sqrt{0.1} = 0.6338$, note the relation $K_{IC} = \sqrt{EG_C}$). This indicates the FBD model is unsuitable for measuring fracture toughness. It is noted that small variation is still observed in the peak load P_{C1} among the four cases concerned in the figure, this is caused by a change in the FPZ size with different G_C. The variation, however, is reasonably small, and the difference tends to vanish as G_C further decreases, bringing the results closer in line with Equation 1.

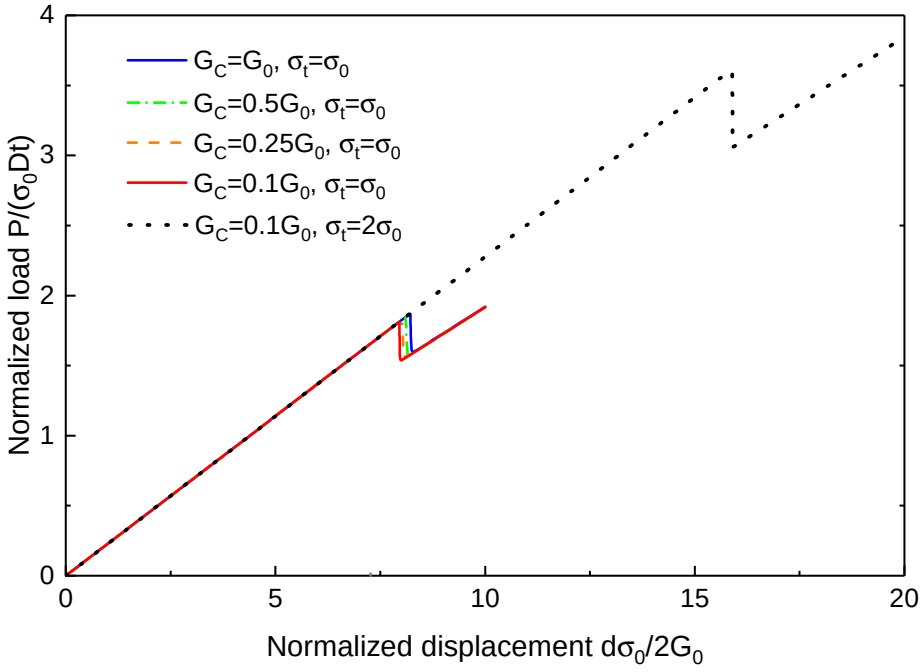

Fig. 7 Loading curves of the FBD specimen with different cohesive parameters. The parameters are normalized using the reference case G_0 and σ_0.

As mentioned, Equation 3 and Fig. 3 predict that P_{C2} can be as low as $0.2P_{C1}$ in an FBD test, which is very hard, if not impossible to obtain in reality. A relatively large drop $P_{C2}/P_{C1} \approx 0.5$ was recorded in [10]. Though

this value is still far larger than expected by LEFM, it is substantially smaller than the lower limit predicted in Fig. 6(b). We suspect this could be due to secondary damage or even loosen loading module during the test, as the load should not be smaller than that at complete failure. As a further step, we took the CZM case with $\sigma_t = \sigma_0$ and $G_C = 0.1G_0$ as an example, as it has the smallest FPZ size and thus best represents LEFM [16]. We tracked the crack propagation to $a = 0.73R$ as shown in Fig. 8(a), which possesses the largest dimensionless stress intensity factor and should correspond to P_{C2} on the loading curve, as indicated by Equation 3 and Fig. 3. The applied stress intensity factor at this stage was evaluated as $K_{app} = 1.17MPa\sqrt{m}$, which is far larger than the intrinsic fracture toughness defined in CZM, $K_{IC} = K_{CZM} = 0.34MPa\sqrt{m}$. Therefore, the basic assumption for the FBD model

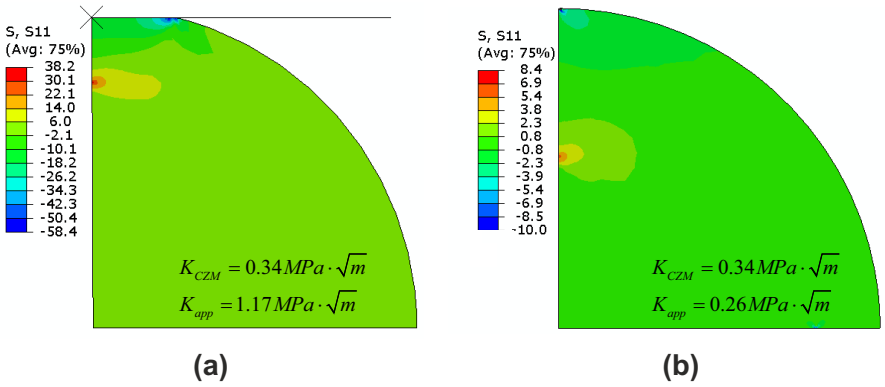

Fig. 8 The stress contour and calculated K_{app} for (a) the FBD specimen at $a = 0.73R$ with the theoretically maximum dimensionless stress intensity factor and (b) the SCB specimen immediately after crack initiation.

that $K_{app} = K_{IC}$ holds during the crack propagation [10] isn't true. Actually, even at the peak in Fig. 3 ($a = 0.73R$) which indicates the transition from unstable to stable crack propagation [10], $K_{app} \approx 3K_{IC}$ so crack propagation

is still highly dynamic. Therefore, the crack keeps extending until complete failure and this "turning" point ($a = 0.73R$) is actually not captured on the loading curve. These are the problems that undermine the accuracy of the FBD model in the measurement of the fracture toughness. In 1993, Guo et al. [3] proposed a method for measuring mode I fracture toughness using a full Brazilian disk without a pre-crack; the formulation was very similar to the FBD test. Zhao et al. [31] wrote a discussion on this method and expressed similar concern, which is cited here: *"... the stored strain energy for the uncracked disk at the failure initiation point is far more than the energy needed to fracture the sample; therefore, it is suspected that second lower point on the loading curve is NOT corresponding to the maximum stress intensity factor, but corresponds to the situation where the sample had already broken into two halves. Because of restriction by the jaws on the disk, the two broken halves can still stay in position to take the external load."* This seems to be supported by our observation. It should be mentioned that cohesive zone simulations were only performed on the standard flattened Brazilian disk tests, but we didn't actually simulate the conventional Brazilian disk tests.

With CZM, we quantitatively studied the energetics during crack propagation. A well known issue with CZM is its numerical divergence at crack initiation, which interrupts the simulation. This was carefully studied by Yu et al. [15] taking a bilinear TSL. Using a two element model, it was shown that the divergence was caused by a so-called snap-back issue in a uniaxial tension scenario. A solution could be using the Riks method or enforcing the local crack tip displacement as proposed in [32, 33] so that the remote displacement can decrease when failure initiates. Such approaches are suit-

able if the purpose of the simulation is to capture the post-failure behaviour of the structure. In a constant displacement scenario, divergence occurs due to the existence of several solutions at failure causing numerical instability. Energetically, in both cases the strain energy released by the structure during failure is larger than the energy that can be consumed by the cohesive elements. Take the snap-back case for instance, the total strain energy is zero at complete failure, releasing all the stored energy, the remote displacement therefore tends to reduce so that some strain energy is maintained and the release matches cohesive consumption. Following this idea, a viscous regularization scheme is often applied to compensate for the excess in available energy, with the formulation detailed in [15]. Numerically this part of energy is classified as viscous dissipation, in reality it could represent the part of energy consumed due to dynamic effects, such as dynamic wave propagation in the matrix.

The same issue was encountered when modelling the FBD test. In Fig. 5 the failure displacement is around $0.82mm$. The strain energy release at complete failure assuming negligible change in the displacement can be easily extracted using the two simple cases in Fig. 6, $\approx 0.48N \cdot m$. The total cohesive energy consumption at complete failure, taking the approximate value $K_{IC} = 1.1MPa\sqrt{m}$ in Fig. 5, is only $\approx 0.19N \cdot m$. We therefore used the viscous regularization method to dissipate the extra released energy in the CZM simulation. The failure load is unaffected as long as the applied viscosity coefficient is sufficiently small, which was determined via a convergence study. The energy evolution for the case $\sigma_C = \sigma_0, G_C = 0.1G_0$ in Fig. 7 is plotted in Fig. 9(a). The viscous dissipation is close to 20 times as large

as the cohesive energy consumption during failure, meaning that the crack propagation is highly dynamic during the entire failure process, so that the theoretical maximum point of dimensionless stress intensity factor in Fig. 3 cannot be properly captured.

So far, it can be concluded that Equation 3 is unsuitable for extracting the fracture toughness. This equation is theoretically correct, but 1) the FBD geometry gives a very small window for the variation of P_{C2} such that P_{C2} is practically insensitive to the change in the fracture toughness and 2) the crack propagation from the uncracked specimen is highly dynamic so the theoretical turning point cannot be measured in practice. Meanwhile, it should be noted that the FBD model works well in predicting the tensile strength. This is verified by simulating a further case with $\sigma_C = 2\sigma_0, G_C = 0.1G_0$ as shown in Fig. 7. The first peak P_{C1} doubled with the fracture strength, and the exact value agrees well with Equation 1.

4.2. The SCB model

Now that it is not possible to calibrate both the tensile strength and fracture toughness within a single test, we need a separate experiment to measure the fracture toughness. According to Zhao et al. [31], the tests on pre-cracked specimens are likely to give more accurate prediction. The CCNBD test and the SCB test are within this category. Compared with the conventional pre-notched three point bending test, these methods benefit from simpler sample preparation and a larger failure load which gives higher accuracy. Here we take the SCB model as an example and study it with CZM for two purpose, to verify its effectiveness for our future tests and to further contrast it with the FBD model.

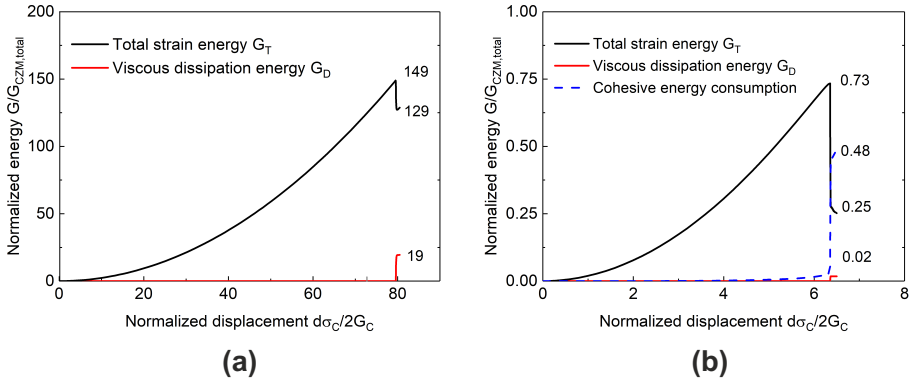

Fig. 9 The evolution of energies during failure in the (a) FBD specimen and (b) SCB specimen, for the case $G_C = 0.1G_0$ and $\sigma_C = 0.1\sigma_0$ which is the most representative of the LEFM case. The energy is normalized by the total cohesive energy at complete separation of the specimen, $G_{CZM,total} = G_C \cdot A_{CZM}$ with A_{CZM} being the total area of the cohesive interface. It is noted that the cohesive consumption is ≈ 1 in (a) but is overshadowed by other curves.

As shown in Fig. 2(b), the radius of the disk was selected as $R = 50mm$, the span $2s = 80mm$ and the thickness $t = 50mm$. A pre-crack with length $a = 0.5R$ was introduced. Due to symmetry, a half of the disk was modelled in ABAQUS, assuming plane strain condition. The central ligament was modelled with cohesive elements with a fine mesh resolution. The entire model has 1914 plane strain elements and 180 cohesive elements.

We took the same five combinations of cohesive parameters as presented in Fig. 7 and plotted the simulated loading curves in Fig. 10. The variation in G_C and thus in K_{IC} are captured very well. Among these, the case with $\sigma_t = \sigma_0, G_C = 0.1G_0$ and the case with $\sigma_t = \sigma_0, G_C = 0.25G_0$ are the most representative of the LEFM results, we had $P_{max} = 870N$ in the former and $P_{max} = 1300N$ in the latter, and the ratio between these two is 0.67, very close to the expectation of Equation 4, $1/\sqrt{2.5} = 0.63$. Further, taking

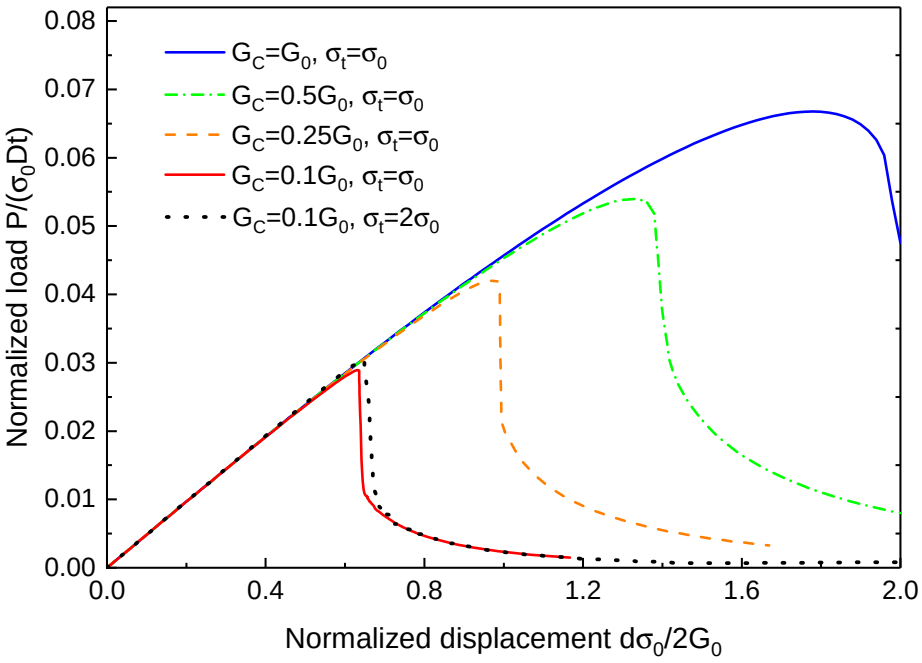

Fig. 10 Loading curves of the SCB specimen with different cohesive parameters. The parameters are normalized using the reference case G_0 and σ_0.

$P_{max} = 870N$ into Equation 4 and according to the coefficients provided by Kuruppu et al. [9], the fracture toughness extracted from the loading curve is $K_{IC} = 0.32MPa\sqrt{m}$, which is in good agreement with that converted directly from the cohesive parameters $G_C = 0.1G_0 \rightarrow K_C = 0.34MPa\sqrt{m}$. These prove that the SCB model gives satisfactory prediction of the fracture toughness.

The SCB model (Equation 4) was derived based on a similar procedure as the FBD model also assuming $K_{app} = K_{IC}$ at failure. We took the moment when the crack starts to propagate in the SCB specimen as illustrated in Fig. 8(b) and evaluated the applied stress intensity factor

$K_{app} = 0.26MPa\sqrt{m}$. In contrast to the FBD model where K_{app} is substantially larger than K_{IC}, the assumption that $K_{app} = K_{IC}$ approximately holds in the SCB model. This indicates that the assumption of quasi-static crack propagation holds, at least at the beginning of crack propagation in this model. Similarly, we plotted the evolution of energies during failure in the SCB simulation in Fig. 9(b). The released strain energy in this test is mainly consumed by the cohesive zone, with marginal viscous dissipation/dynamic effect. This is further evidence that the crack propagation can be regarded as quasi-static in this model and so the assumption of $K_{app} = K_{IC}$ is appropriate.

We further simulated the case with $\sigma_t = 2\sigma_0, G_C = 0.1G_0$ and included the loading curve in Fig. 10. Apparently, the SCB model cannot distinguish the difference in the tensile strength given the same fracture toughness. This is sensible as the crack tip stress field is theoretically singular according to LEFM and the change in tensile strength makes little difference to crack propagation.

5. Summary

Triggered by an inconsistency observed in the FBD tests on pre-baked carbon, we re-examined the applicability of the FBD geometry in measuring mode I fracture toughness. CZM was employed to simulate the test data and to revisit the FBD model. It was found that the tensile strength could be properly calibrated by the FBD model using the maximum load P_{C1} corresponding to crack initiation. However, this model is unsuitable for calibrating the fracture toughness due to the following reasons:

(I) Although theoretically correct, the FBD geometry gives a very narrow window for the variation of the load: under the condition that the displacement keeps constant during failure, which is true for the test, the lowest possible load after failure is just $P_{C2} = 85\%P_{C1}$. So P_{C2} is insufficient to capture the change in K_{IC} which can easily vary by $> 15\%$ among different materials.

(II) Due to the absence of a pre-crack, the stored strain energy is much higher than that can be consumed by the creation of new free surfaces, this makes the crack propagation highly unstable and dynamic throughout failure. P_{C2} corresponds to complete failure of the specimen in reality instead of to the theoretical maximum dimensionless stress intensity factor in Fig. 3. In other words, $K_{app} = K_{IC}$ does NOT hold throughout the test, therefore the LEFM based equation should not be used to extract K_{IC}.

We further verified the effectiveness of the SCB test in measuring the fracture toughness. Due to the existence of a pre-crack in this model, the stored strain energy is lower and comparable to that can be consumed by static crack propagation, such that dynamic effect is marginal and $K_{app} = K_{IC}$ holds approximately at crack propagation. This makes the SCB test a feasible approach to calibrating the mode I fracture toughness. As expected, the SCB model was found unsuitable to extracting the tensile strength of the material.

The conclusions could be projected beyond the current results. Generally speaking, the FBD model is to some extent representative of disk compression tests without introducing a pre-crack, e.g. the full Brazilian disk test [3],

and the SCB model of pre-cracked disk compression tests e.g. the CCNBD test [6], another method recommended by ISRM. The former seems more suitable for measuring the tensile strength from P_{C1} and the latter for measuring the fracture toughness from P_{max}. These peak points are reliable as they are the conversion point from quasi-static loading to (possibly dynamic) failure, so the statically based strength theory and LEFM theory still apply. The usage of the so-called second turning point after failure, e.g. P_{C2} to extract mechanical properties should be examined carefully, as it may bring in dynamic effect. These provide useful clues for the selection and development of test methods.

Acknowledgements

H.Y. wishes to thank Dr. Emilio Martínez Pañeda for the informative discussion on the modelling of Brazilian disk, especially on the convergence problem in CZM.

References

[1] L. Tutluoglu, C. Keles, Mode i fracture toughness determination with straight notched disk bending method, International Journal of Rock Mechanics and Mining Sciences 48 (2011) 1248–1261.

[2] G. Hondros, The evaluation of poisson's ratio and the modulus of materials of low tensile resistance by the brazilian (indirect tensile) test with particular reference to concrete, Australian J. Appl. Sci. 10 (1959) 243–268.

[3] H. Guo, N. I. Aziz, L. C. Schmidt, Rock fracture-toughness determination by the brazilian test, Engineering Geology 33 (1993) 177–188. Cited By :57 Export Date: 22 December 2015.

[4] Q.-Z. Wang, L. Xing, Determination of fracture toughness kic by using the flattened brazilian disk specimen for rocks, Engineering Fracture Mechanics 64 (1999) 193–201.

[5] B. V. D. Steen, A. Vervoort, J. A. L. Napier, Observed and simulated fracture pattern in diametrically loaded discs of rock material, International Journal of Fracture 131 (2005) 35–52.

[6] R. J. Fowell, C. Xu, The use of the cracked brazilian disc geometry for rock fracture investigations, International Journal of Rock Mechanics and Mining Sciences & Geomechanics Abstracts 31 (1994) 571–579.

[7] R. J. Fowell, Suggested method for determining mode i fracture toughness using cracked chevron notched brazilian disc (ccnbd) specimens, International Journal of Rock Mechanics and Mining Sciences & Geomechanics Abstracts 32 (1995) 57–64.

[8] Q. Z. Wang, X. P. Gou, H. Fan, The minimum dimensionless stress intensity factor and its upper bound for ccnbd fracture toughness specimen analyzed with straight through crack assumption, Engineering Fracture Mechanics 82 (2012) 1–8.

[9] M. D. Kuruppu, Y. Obara, M. R. Ayatollahi, K. P. Chong, T. Funatsu, Isrm-suggested method for determining the mode i static fracture tough-

ness using semi-circular bend specimen, Rock Mechanics and Rock Engineering 47 (2014) 267–274.

[10] Q. Z. Wang, X. M. Jia, S. Q. Kou, Z. X. Zhang, P. A. Lindqvist, The flattened brazilian disc specimen used for testing elastic modulus, tensile strength and fracture toughness of brittle rocks: analytical and numerical results, International Journal of Rock Mechanics and Mining Sciences 41 (2004) 245–253.

[11] R. J. Fowell, C. Xu, P. A. Dowd, An update on the fracture toughness testing methods related to the cracked chevron-notched brazilian disk (ccnbd) specimen, pure and applied geophysics 163 (2006) 1047–1057.

[12] Y. G. Huang, L. G. Wang, Y. L. Lu, J. R. Chen, J. H. Zhang, Semi-analytical and numerical studies on the flattened brazilian splitting test used for measuring the indirect tensile strength of rocks, Rock Mechanics and Rock Engineering 48 (2015) 1849–1866.

[13] S. Wu, J. Ma, Y. Cheng, M. Xu, X. Huang, Numerical analysis of the flattened brazilian test: Failure process, recommended geometric parameters and loading conditions, Engineering Fracture Mechanics 204 (2018) 288–305.

[14] C. Keles, L. Tutluoglu, Investigation of proper specimen geometry for mode i fracture toughness testing with flattened brazilian disc method, International Journal of Fracture 169 (2011) 61–75.

[15] H. Yu, J. S. Olsen, V. Olden, A. Alvaro, J. He, Z. Zhang, Viscous regularization for cohesive zone modeling under constant displacement: An

application to hydrogen embrittlement simulation, Engineering Fracture Mechanics 166 (2016) 23–42.

[16] Z. H. Jin, C. T. Sun, A comparison of cohesive zone modeling and classical fracture mechanics based on near tip stress field, International Journal of Solids and Structures 43 (2006) 1047–1060.

[17] J. T. Wang, Relating cohesive zone model to linear elastic fracture mechanics (2010).

[18] Q. Z. Wang, L. Z. Wu, The flattened brazilian disc specimen used for determining elastic modulus, tensile strength and fracture toughness of brittle rocks: experimental results, International Journal of Rock Mechanics and Mining Sciences 41, Supplement 1 (2004) 26–30.

[19] M. D. Kuruppu, K. P. Chong, Fracture toughness testing of brittle materials using semi-circular bend (scb) specimen, Engineering Fracture Mechanics 91 (2012) 133–150.

[20] H. Yu, J. S. Olsen, V. Olden, A. Alvaro, J. He, Z. Zhang, Cohesive zone simulation of grain size and misorientation effects on hydrogen embrittlement in nickel, Engineering Failure Analysis 81 (2017) 79–93.

[21] H. Khoramishad, J. Akbardoost, M. Ayatollahi, Size effects on parameters of cohesive zone model in mode i fracture of limestone, International Journal of Damage Mechanics (2013).

[22] P. W. Harper, S. R. Hallett, Cohesive zone length in numerical simulations of composite delamination, Engineering Fracture Mechanics 75 (2008) 4774–4792.

[23] A. Turon, C. G. Dávila, P. P. Camanho, J. Costa, An engineering solution for mesh size effects in the simulation of delamination using cohesive zone models, Engineering Fracture Mechanics 74 (2007) 1665–1682.

[24] C.-Y. Hui, J. A., S. J. Bennison, J. D. Londono, Crack blunting and the strength of soft elastic solids, Proceedings of the Royal Society of London. Series A: Mathematical, Physical and Engineering Sciences 459 (2003) 1489–1516.

[25] J. Reinoso, P. Durand, P. R. Budarapu, M. Paggi, Crack patterns in heterogenous rocks using a combined phase field-cohesive interface modeling approach: A numerical study, Energies 12 (2019) 965.

[26] C. Miehe, M. Hofacker, F. Welschinger, A phase field model for rate-independent crack propagation: Robust algorithmic implementation based on operator splits, Computer Methods in Applied Mechanics and Engineering 199 (2010) 2765–2778.

[27] D. H. Andersen, Z. L. Zhang, Fracture and physical properties of carbon anodes for the aluminum reduction cell, Engineering Fracture Mechanics 78 (2011) 2998–3016.

[28] Prebaked consumable carbon anodes, https://en.wikipedia.org/wiki/Prebaked_Consumable_Carbon_Anodes, Web Page. Accessed: 2020-04-15.

[29] A. U. Manual, Version 6.14-1, Dassault Systémes Simulia Corp., Providence, RI (2014).

[30] H. Yu, J. S. Olsen, A. Alvaro, V. Olden, J. He, Z. Zhang, A uniform hydrogen degradation law for high strength steels, Engineering Fracture Mechanics 157 (2016) 56–71.

[31] X. L. Zhao, R. J. Fowell, J. C. Roegiers, C. Xu, Rock fracture-toughness determination by the brazilian test, by h. guo, n.i. aziz, l.c. schmidt, Engineering Geology 38 (1994) 181–184.

[32] E. Martínez-Pañeda, S. del Busto, C. Betegón, Non-local plasticity effects on notch fracture mechanics, Theoretical and Applied Fracture Mechanics 92 (2017) 276–287.

[33] L. García-Guzmán, J. Reinoso, A. Valverde-González, E. Martínez-Pañeda, L. Távara, Numerical study of interface cracking in composite structures using a novel geometrically nonlinear linear elastic brittle interface model: Mixed-mode fracture conditions and application to structured interfaces, Composite Structures 248 (2020) 112495.